INSTITUTE OF PHYSICS PUBLISHING MEASUREMENT SCIENCE AND TECHNOLOGY

Meas. Sci. Technol. **18** (2007) 404–414 doi:10.1088/0957-0233/18/2/S12

A landmark-based 3D calibration strategy for SPM

Martin Ritter[1], **Thorsten Dziomba**[2], **Axel Kranzmann**[1] **and Ludger Koenders**[2]

[1] Bundesanstalt für Materialforschung und -prüfung, Unter den Eichen 87, 12205 Berlin, Germany
[2] Physikalisch-Technische Bundesanstalt Braunschweig und Berlin, Bundesallee 100, 38116 Braunschweig, Germany

E-mail: Martin.Ritter@bam.de

Received 30 May 2006, in final form 10 October 2006
Published 12 January 2007
Online at stacks.iop.org/MST/18/404

Abstract

We present a new method for the complete three-dimensional (3D) calibration of scanning probe microscopes (SPM) and other high-resolution microscopes, e.g., scanning electron microscopes (SEM) and confocal laser scanning microscopes (CLSM), by applying a 3D micrometre-sized reference structure with the shape of a cascade slope-step pyramid. The 3D reference structure was produced by focused ion beam induced metal deposition. In contrast to pitch featured calibration procedures that require separate lateral and vertical reference standards such as gratings and step height structures, the new method includes the use of landmarks, which are well established in calibration and measurement tasks on a larger scale. However, the landmarks applied to the new 3D reference structures are of sub-micrometre size, the so-called 'nanomarkers'. The nanomarker coordinates are used for a geometrical calibration of the scanning process of SPM as well as of other instrument types such as SEM and CLSM. For that purpose, a parameter estimation routine involving three scale factors and three coupling factors has been developed that allows lateral and vertical calibration in only one sampling step. With this new calibration strategy, we are able to detect deviations of SPM lateral scaling errors as well as coupling effects causing, e.g., a lateral coordinate shift depending on the measured height position of the probe.

Keywords: scanning probe microscopy, focused ion beam, calibration, 3D standards, parameter estimation, spatial coupling, distortions

1. Introduction

A major contribution to the success of technologies and research in the micro- and nanometre range is marked by the ability to visualize small features and to measure at this scale. Together with the confocal laser scanning microscope (CLSM) and the scanning electron microscope (SEM), the scanning probe microscope (SPM) belongs to the most common measurement and imaging tools applied in research, quality assurance and metrology at the micro-range and below for spatial analysis [1–3]. SPM and CLSM allow direct spatial coordinate measurements. In the case of SEM, the spatial information has to be reconstructed indirectly from a series of 2D images, e.g., by photogrammetric means [4–6].

Although scanning microscopes are still often only used for the sake of visualization and qualitative analysis, they are increasingly applied for quantitative 3D measurements as well. This is the case especially in the field of nanotechnology, where dimensional metrology aspects of measurements are critical [7], or even a prerequisite for successful fabrication control of nano-structures [8]. However, establishing coordinate measurement devices for the micro-scale and nano-range that are directly traceable to the metre requires effort, technology, knowledge and infrastructure that often only National Metrology Institutes (NMIs), e.g. PTB in Germany, NIST in the USA, NPL in the United Kingdom, NMIJ in Japan, and a few others can provide and afford. Therefore, most of the

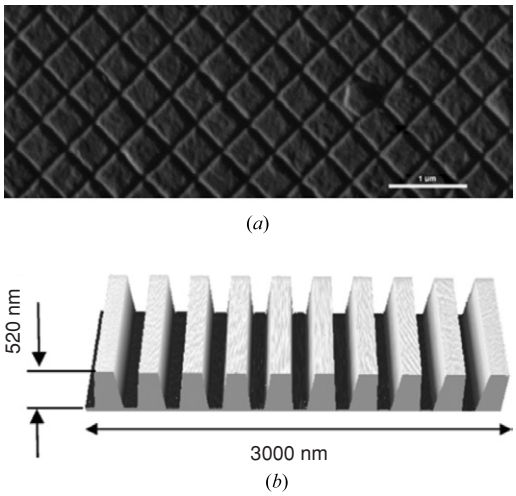

Figure 1. Typical 1D and 2D reference structures for (*a*) lateral and (*b*) vertical scale calibration of scanning microscopes.

commercial scanning microscopes that are operated in research and in industrial facilities are calibrated by physical transfer standards, instead. The fabrication of such highly accurate dimensional standards for that scale is a challenge, and the calibration procedure itself has to be considered carefully [9].

While for CLSM, a few more or less suited dimensional transfer standards are available, SEM magnification and distortions are usually calibrated by imaging small orthogonal gratings such as the one shown in figure 1(*a*) [10]. For SPMs, up to now a variety of dimensional standards has been developed [11], and most are commercially available from a number of companies worldwide [12]. The characteristic common to all standards for 3D scanning microscopy at the micro- and nano-ranges is that they are primarily intended either for lateral or vertical calibration: 1D or 2D repetitive structures in the lateral direction, such as 2D gratings (figure 1(*a*)) of good homogeneity whose pitch value is used for the lateral calibration, or in the vertical direction, 1D height steps (figure 1(*b*)) for *z*-axis calibration of the scale.

A special flatness standard, e.g. for the determination of SPM scan-bows and the characterization of other deviations from perfect plane movement, has also been developed [11].

Here, an alternative landmark-based geometrical calibration strategy generally suited for a variety of scanning microscopy techniques is introduced. It uses 3D reference structures in contrast to the existing 1D and 2D pitch standards (for the calibration of the lateral axes), or 1D step height standards (for the calibration of the vertical axis). The fabrication of the presented 3D microstructures is accomplished by focused ion beam (FIB) induced metal deposition [13]. On the 3D reference structures, the so-called nanomarkers are applied that serve as landmarks (control points) with distinct 3D coordinates. Unlike established calibration methods, this approach not only allows the calibration of scanning microscopes in one step (one-step 3D calibration), without decoupling the lateral from the height calibration, but also provides the opportunity to perform coordinate measurements that are almost independent of the peculiarities of the given 3D scanning techniques. This advantage ensures a broad versatility and, moreover,

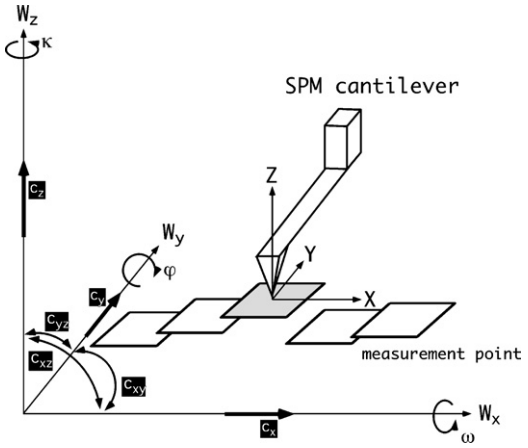

Figure 2. SPM scanning movement with reference coordinate system **x** and measurement coordinate system **w**.

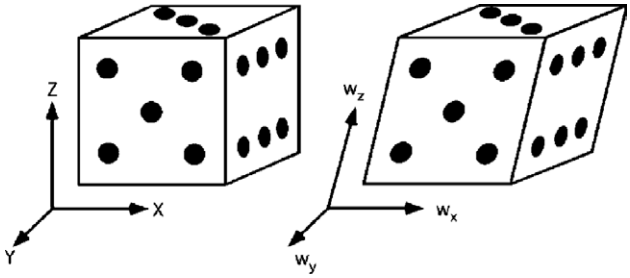

Figure 3. Linear geometric distortions in 3D measurement due to skewed measurement (scan) coordinate system **w**.

enables a correlative analysis of the individual nanomarker coordinate measurements by the various microscopes. The ability to systematically compare the imaging performance of microscopes based on different imaging or measurement techniques by using landmarks is very powerful for an error analysis. Such error separation by correlative analysis is often the only practical way to identify and quantify guidance errors and other distortions of the individual instruments, as this separation based on correlation allows geometrical distortions to be clearly linked to specific devices (see section 5.2).

2. Principle of 3D landmark-based geometrical SPM calibration

2.1. Established SPM calibration procedures

The geometric calibration of scanning microscopes is necessary to achieve accurate dimensional measurements. A great deal of systematic error introduced into the measurement comes from imperfections of the scanning system [14]. An ideal scanning movement (figure 2) forms a coordinate system **x** with orthogonal scanning axes and constant step sizes in all directions. The actual accomplished, usually non-ideal scanning movement forms the measurement coordinate system **w** that is only an approximation to that ideal, simply because of limitations of the hardware performing the scan (figure 3). An overview of possible distortion factors not only due to hardware errors, but also due to external factors, such as thermal drift, is given in [15, 16].

Currently, the calibration of SPM is usually performed by separate determinations of the correction parameters for

lateral and vertical scales. Eventually, additional correction parameters are determined for nonlinearity and coupling of the lateral axes [17]. Separate SPM reference standards exist for the calibration of lateral and vertical scales of SPM instruments. They consist of 1D or 2D pitch standards for the lateral calibration, with an actual pitch from a few nanometres to several micrometres (figure 1(*a*)), or of 1D elevations with a step height up to several micrometres for vertical calibration (figure 1(*b*)). The determination of the vertical correction parameter is performed with the help of reference structures of a very consistent step height as shown in figure 1(*b*). The height of the step in the measurement is determined either by a histogram analysis or by the ISO 5436 method [9].

The lateral geometrical calibration of the SPM, at least, has to yield linear scale correction factors. Furthermore, it should consider distortions in the scanning movement by higher order scale correction factors, and eventually take the non-orthogonality of the *x*- and *y*-axes of the scanning system into account by introducing a coupling factor. Hence, for the lateral calibration with 2D gratings, Jørgensen *et al* [17] propose a transformation model for the description of the correspondence of the measured lattice and the real lattice. In order to reconstitute the lattice coordinates from the observed data, an affine transformation model is chosen with two scaling factors in the *x*- and *y*-directions (c_x, c_y) and a coupling factor for the description of shearing between the *x*- and *y*-axes (c_{xy}), i.e. the deviation from the perpendicular. The corresponding coordinate pairs are determined by the formation of a unit cell representing the smallest repetitive part of the measured grating and an ideal grating formed by the actual pitch of the grating.

Therefore, highly analogous to the standard design of the SPM itself, the commonly applied model for the calibration procedure decouples the estimation of the lateral correction factors from the determination of the vertical correction factors.

Such a calibration procedure has major drawbacks. It has to be considered that the calibration process involving the separate determination of the correction factors for the lateral and vertical dimensions is rather time consuming. Most critically, it may be hard to detect local correlations between the vertical measurement and the lateral data, when separating the calibration routine into two independent calibration steps, although this is possible in principle [18]. In other words, by separating the calibration into a lateral and a vertical step, the determination of the *z*-correction factor is an averaging process that is independent of the lateral scanning position, a situation that is not given in actual measurements.

2.2. Landmark-based 3D calibration

We show that an integrated model for 3D calibration is possible in one step and models the geometry of the scanning process more accurately because the calibration routines need not be separated. This alternative approach uses 3D reference structures with known object coordinates, e.g. landmarks, to determine geometric distortions of the scan process. Landmarks are also called control points or fiducial marks, and are here referred to as nanomarkers, due to their

(*a*)

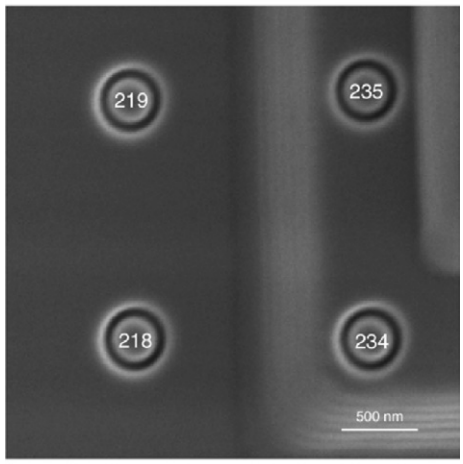

(*b*)

Figure 4. Landmark examples applied at two different scales. (*a*) Terrestrial landmarks and (*b*) 'nanomarkers' at the micro-range.

sub-micrometre size. In general, they are unambiguous, easily recognizable, geometrical features on real objects that define image coordinates in 2D or object coordinates in 3D measurement data. Because landmarks define discrete positions on a real object, they are widely used for coordinate measurements in geoinformation sciences (figure 4(*a*)), by engineers, e.g. for the study of the dynamic behaviour of construction components, in the sport sciences to trace body movements and also for calibration purposes in close-range applications [19]. The use of landmarks for micro-range measurements and below is established here (figure 4(*b*)), although a few specific applications have been reported in the past, such as for quality control of SPM cantilevers [20], for the photogrammetric calibration of an SEM [21] and for medical applications, e.g. for the registration of computer tomography images of the head in order to allow microsurgery [22].

Several geometries of such features are possible. Often, circles are applied (figure 4(*a*)), in which the perimeter depicts the chosen geometrical feature of the landmark and the centre maps the control point coordinates in measurements or 2D images. We also chose a ring-shaped variant (figure 4(*b*)) for clearer identification in the measurement, or image processing data, as described in section 4.2.

By means of SPM, the object coordinates of each nanomarker are determined with low uncertainty. The uncertainty of the nanomarker position measurements may be reduced even further by making use of a correlative analysis, i.e. a comparative evaluation of the measurement results obtained by different measurement techniques as described in section 5.2. The 3D coordinates of the nanomarkers—as determined by these calibration measurements—are then used as reference data for the calibration of the scale and coupling factors of various users' instruments.

Figure 3 demonstrates spatial linear distortion effects on a simple geometric structure due to imperfections of the scan generator. What would originally be a cube in the reference coordinate system **x** is skewed and has become a parallelepiped, due to a distorted measurement coordinate system **w**.

In order to restore the original 3D shape of the cube in the measurement, the measurement coordinate system **w** has to be transformed to the reference coordinate system **x** by including translation, rotation, non-isotropic scaling and shearing, as shown in equation (1):

$$\mathbf{x} = \mathbf{R} \cdot \mathbf{M} \cdot \mathbf{S} \cdot \mathbf{w} + \mathbf{t}. \tag{1}$$

This is achieved by a least-squares parameter estimation where the measured object coordinates **w** (w_x, w_y, w_z) are registered to the known object coordinates **x** (X, Y, Z), i.e. to the reference data as usually determined by metrology SPM. The registration of the two coordinate measurements can be achieved by a geometric transformation including a rigid movement that consists of a rotation in space **R** and a translation **t**, a non-isotropic scaling in all directions by **M** (c_x, c_y, c_z) and an affine coupling (shearing) **S** (c_{xy}, c_{xz}, c_{yz}) (equation (2)). The parameters of **M** and **S** obtained in our case are the linear correction factors for the geometrical calibration

$$\begin{bmatrix} x \\ y \\ z \end{bmatrix} = \begin{bmatrix} r_1 & r_2 & r_3 \\ r_4 & r_5 & r_6 \\ r_7 & r_8 & r_9 \end{bmatrix} \begin{bmatrix} c_x & 0 & 0 \\ 0 & c_y & 0 \\ 0 & 0 & c_z \end{bmatrix} \begin{bmatrix} 1 & c_{xy} & c_{xz} \\ 0 & 1 & c_{yz} \\ 0 & 0 & 1 \end{bmatrix} \begin{bmatrix} w_x \\ w_y \\ w_z \end{bmatrix} + \begin{bmatrix} t_x \\ t_y \\ t_z \end{bmatrix}. \tag{2}$$

In order to be able to perform the least-squares parameter estimation for the determination of the linear geometrical correction factors, corresponding points in the measurement coordinate system **w** and in the reference coordinate system **x** have to be available. These homologous object coordinates are provided by the nanomarkers. The benefit of the coordinate registration is visible by the resulting mean point error ξ_p, which is a by-product of the least-squares parameter estimation, usually derived from the square root of the weighted residues. For descriptive purposes, equation (3) shows the determination of the mean point error in the non-weighted case. It can be seen that a decrease in ξ_p generally indicates smaller residues after estimation, and therefore a more accurate description of the calibration model:

$$\xi_p = \frac{1}{n} \sum_{i=1}^{n} \sqrt{(x_i - w_{xi})^2 + (y_i - w_{yi})^2 + (z_i - w_{zi})^2}. \tag{3}$$

This explains the importance of the possibility of uniquely determining the nanomarkers by their special arrangement and denotation (see section 4.2 and figure 7). The 3D reference structure itself only serves as the spatial carrier of the landmarks, up to now.

3. 3D reference structure fabrication and design

3.1. 3D reference structure fabrication by focused ion beam

As a method for the fabrication of the 3D microstructures, we chose FIB gas-induced metal deposition. The FIB technology allows the flexible fabrication of versatile spatial objects [23] in order to fit best the needs for the chosen microscopy technique. FIB systems work similarly to SEM, but their capabilities go far beyond imaging [23]. The biggest difference between FIB and SEM is the use of an ion beam instead of an electron beam. Because ions are much larger and heavier than electrons, other characteristics of sample interaction and imaging apply. In particular, the high momentum of the ions is transferred to the sample atoms within a short distance. The resulting speed and energy are high enough to remove the sample atoms from the surrounding matrix. This process is called milling and can be deliberately applied for the fabrication of micro- and nano-structures [24].

Alternatively, in the controlled presence of an organo-metallic gas within the specimen chamber, the ions of the beam interact with the gas adsorbed on the sample surface. Thereby, the gas is decomposed into a volatile organic component and a solid metallic component that attaches to the substrate surface. Continuous decomposition and attachment can be used for a deliberate build-up of micro- and nano-structures. This process is called deposition, or more accurately chemical vapour deposition (CVD) [25].

By controlled milling and deposition at the desired well-defined locations, FIB is a technology of unique versatility to structure or to manipulate samples on a micro- and particularly nano-scale, respectively. Especially milling shows a high aspect ratio and, thereby, even allows to cut ultra-thin slices out of the bulk, e.g., for TEM inspection. Both micro- and nano-fabrication processes are referred to as patterning.

3.2. 3D reference structure design

The peculiarities of the calibration process itself had to be taken into consideration when planning the construction of the 3D micro-calibration object. In general, it is an advantage in 3D measurement methods if the calibration object covers the measurement volume. Therefore, the nominal measures of a 3D calibration object should represent approximately the usual measurement volume; most SPM scanner systems are limited in lateral and vertical movements. They can handle a lateral scan area up to 100 μm × 100 μm with a maximum structure elevation of about 8–12 μm (z-range). A width-to-height ratio of 1/8 for a large horizontal field width (HFW) and 1/5 for small HFW is reasonably followed for experiments. Therefore, the height of each single reference structure, i.e. the structure supporting the nanomarkers, was designed to be approximately within these limits. As the shape of the reference structure, the approved cascade-pyramid layout was chosen [13]. This design allows the creation of nanomarkers not only across the reference field, but also at multiple height levels. Thereby, the SPM measurement volume is optimally

covered, both laterally and vertically. Additionally, the angle of the pyramidal-cascade step slopes with respect to the surface plane is designed to be smaller than the aperture angle of a regular AFM (atomic force microscope) tip, in order to allow safe probing of the pyramidal bodies by AFM with as little influence of tip geometry and distance control artefacts as possible.

3.3. Nanomarker design and alignment

An important task for the landmark-based calibration of scanning microscopes is the choice of suitable nanomarkers as landmarks. This includes the shape of the nanomarkers, their complexity, dimension and depth as design parameters. Especially, they must be easy to detect as discrete features in the SPM data. All of these factors have an influence on the accuracy and reliability of the image coordinate measurement and, therefore, on the calibration accuracy. We tested nanomarkers of different sizes and shapes, e.g., point-shaped nanomarkers, of 30 nm to 50 nm radius. Finally, we chose a ring design (figure 4(*b*)) with a radius of roughly 200 nm in order to be able to perform future correlative measurements with optical microscopes that offer a lower resolution than SPM or SEM. On the other hand, these nanomarkers are still small enough to allow high accuracy calibration of SPM as well.

Besides the substrate, only the flat regions of the pyramids are decorated with the nanomarkers; special care is taken to make sure that no part of the nanomarkers extends into the slope areas of the cascades. In this way, the z-coordinate of the nanomarker is well defined. The required very uniform shape of all nanomarkers is achieved by taking great care that the material properties are the same at all locations where nanomarkers are to be written, by creating them in an automated process so that the same FIB parameters are actually applied for the milling of each nanomarker.

The distribution of the nanomarkers on the lower level of the calibration objects is non-symmetrical (figure 5), so that the user is always informed of the pyramids' orientation. Additionally, this feature allows for the non-ambiguous allocation of the nanomarkers, and thereby the automatic annotation according to a predefined nomenclature (figure 7(*b*)). Furthermore, the nanomarker arrangement pattern is slightly different from pyramid to pyramid in order to ease the safe identification of each pyramid, which are additionally tagged at the base level by larger etched enumeration structures (figures 5 and 6), in order to allow them to be identified automatically by pattern recognition algorithms.

4. SPM measurements and data analysis

4.1. SPM measurements

The investigations of the prototypes of the novel 3D standards discussed here were performed with an optimized commercial scanning force microscope (SIS nc-SFM) in the PTB clean-room centre; a stabilized modified NANOStation II (SIS GmbH, Herzogenrath, Germany). This instrument is based on an Axiotech 100 H (Zeiss) and thereby a combination of an optical microscope and a non-contact SFM, with the AFM head plugged into the turret instead of one of the optical

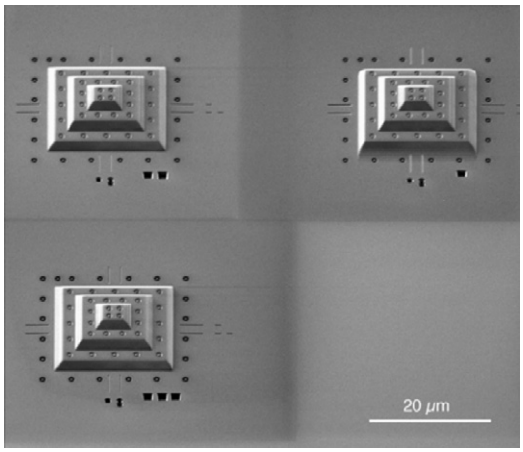

Figure 5. SEM image of a 3D reference structure array (FIB03).

objectives [26]. The advantage of this system is that it allows switching between the optical and AFM modes by simply turning the turret. The cantilever probe can be aligned with the optical axis, e.g., of the 50× optical objective, with a precision of just a few micrometres; the region of interest can thus be easily located and precisely addressed by the probe after sample alignment by means of the optical mode. Such a safe and comfortable navigation on the object is a prerequisite particularly for the detailed investigation of the first prototype arrays of these cascade-pyramid 3D standards. Furthermore, a comparatively large maximum lateral scan range of 109 μm × 109 μm makes this instrument well suited for the studies at these novel standards. The apparatus is housed in an acoustic chamber in the PTB clean-room centre where it is operated under very stable ambient conditions.

While the instrument does not belong to the—often sophisticated—highest traceability class of metrology AFMs (with laser-interferometric position control), it is equipped with a closed-loop capacitive position-controlled xy-piezo scanstage (PI Physik Instrumente, Karlsruhe, Germany) and a piezostack for z-scanning with a strain gauge as a z-sensor.

The instrument is calibrated by transfer standards that have been used in international comparisons and/or that have been certified by PTB's metrology SPMs such as the modified Veritekt [27], or the metrological large-range SPM based on the nano-measuring machine [28]. The metrological properties of the SIS nc-SFM have been characterized in detail and have been constantly monitored for more than 4 years now since the set-up of the instrument. A set of parameter-dependent correction factors has been determined, e.g. scan range and scan rate. They have been taken into account upon the calibration of the lateral axes of the PI scanstage.

For the characterization and preliminary calibration of the novel 3D standards, the following measurement scheme has been followed. First, images of the whole reference field (usually sized 54 μm × 54 μm or 90 μm × 90 μm) containing the array of pyramids have been recorded at 1024 × 1024 pixels. Second, images of higher resolution have been scanned for one-half or one-third of the array, e.g., 20 μm × 60 μm at 1024 × 3036 pixels each, possibly followed by an analysis of a single pyramid or some small individual FIB-created structures. This series of measurements was then

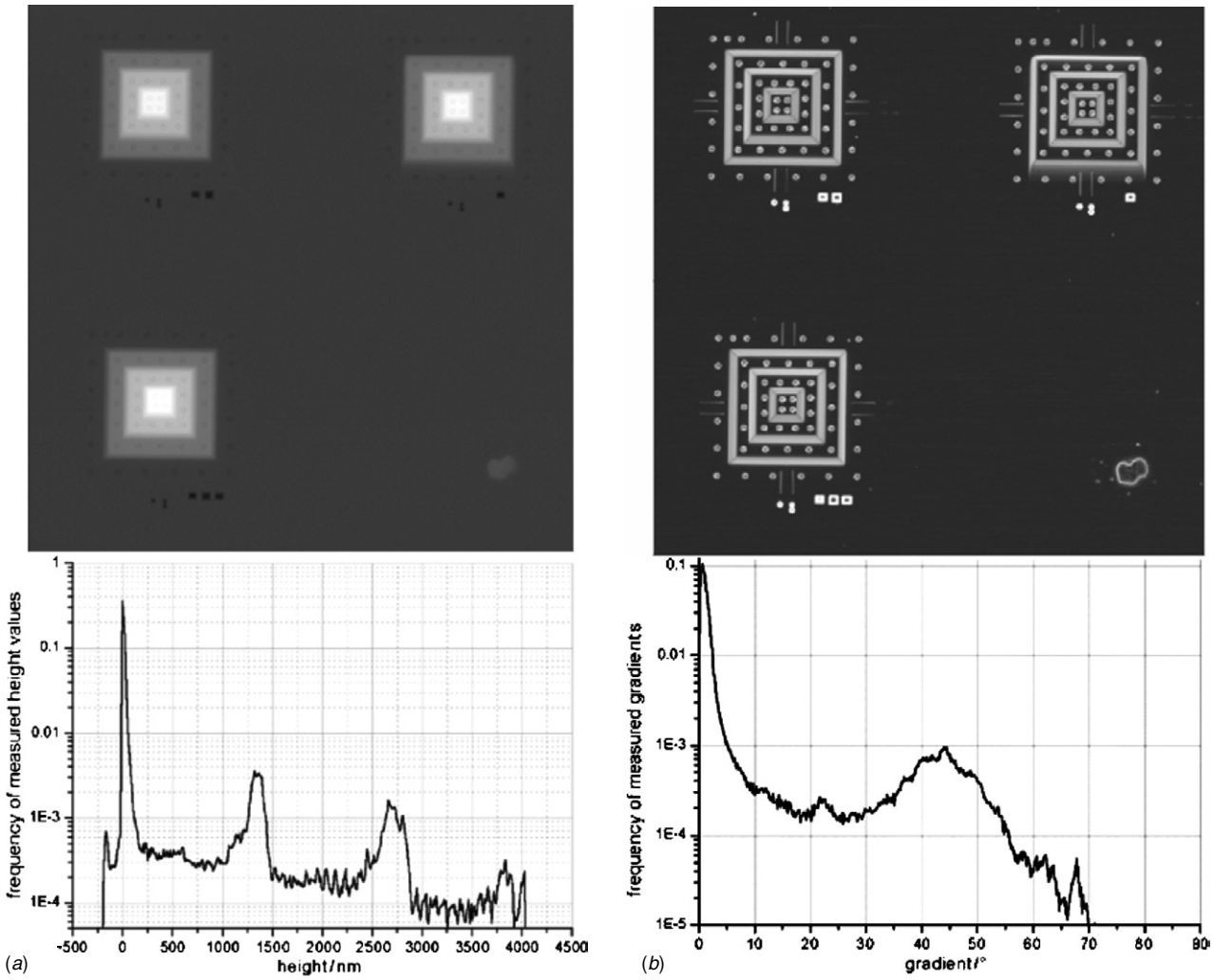

Figure 6. FIB03 array SPM measurement of 90 μm × 90 μm. (*a*) Height measurement with a corresponding histogram showing the three height levels of the pyramids. The zero level is set to the base area; the peak at −200 nm belongs to the enumeration marks, the peak around 1300 nm is the first step, around 2650 nm the second step and the split one around 3800 nm and 4000 nm represents the two—slightly different—top levels of the pyramids, respectively. (*b*) Gradient image of the identical SPM measurement with a gradient histogram showing that the tilt angle of the pyramids is in the range of 40° to 50°. The small peak at 68° represents the much steeper edges of the enumeration marks.

repeated after rotating the sample by 90°. All measurements were recorded with the same parameter settings (scan range, scan rate) under the same measurement conditions (including waiting time, prescans, etc) as those of the instrument calibration.

4.2. Nanomarker coordinate determination

The accuracy of a landmark or control point-based calibration strategy largely depends on the accuracy of the determination of the coordinates of the landmarks from the measurement data. In order to prevent errors introduced by a manual selection of the nanomarker centre coordinates, a strategy using digital image processing routines for the determination of the control point coordinates has been established and utilized. This automation runs fast on any modern computer and thus is more effective than any manual analysis. Figure 7(*a*) illustrates the strategy used for the determination of the landmark coordinates within the micro-range measurement data represented by the nanomarker centre. These data are mainly presented as colour-coded images or, at least, can be transformed into such images. Therefore, image processing methods can be applied to most measurement data, such as, for example, correlation techniques based on template matching, a method that has been preferentially used here for the determination of the nanomarker coordinates. After the user has selected a template nanomarker in the image that has been generated from the measurement data, this template is used to find all lateral nanomarker centre coordinates in the image. By applying this strategy, an uncertainty in coordinate determination of 0.2 to 0.33 of the metric size represented by a pixel or data point could be achieved (not published). In the experiments performed here, averaging or centroiding a 3 × 3 matrix of measurement points has then been used to determine the corresponding z-values of the circle or ring-shaped nanomarker centre coordinates.

For the analysis of the measurement data for calibration purposes, special software using a graphical interface (GUI) has been developed (figure 7(*b*)). With this software, the processing of microscopic images for coordinate

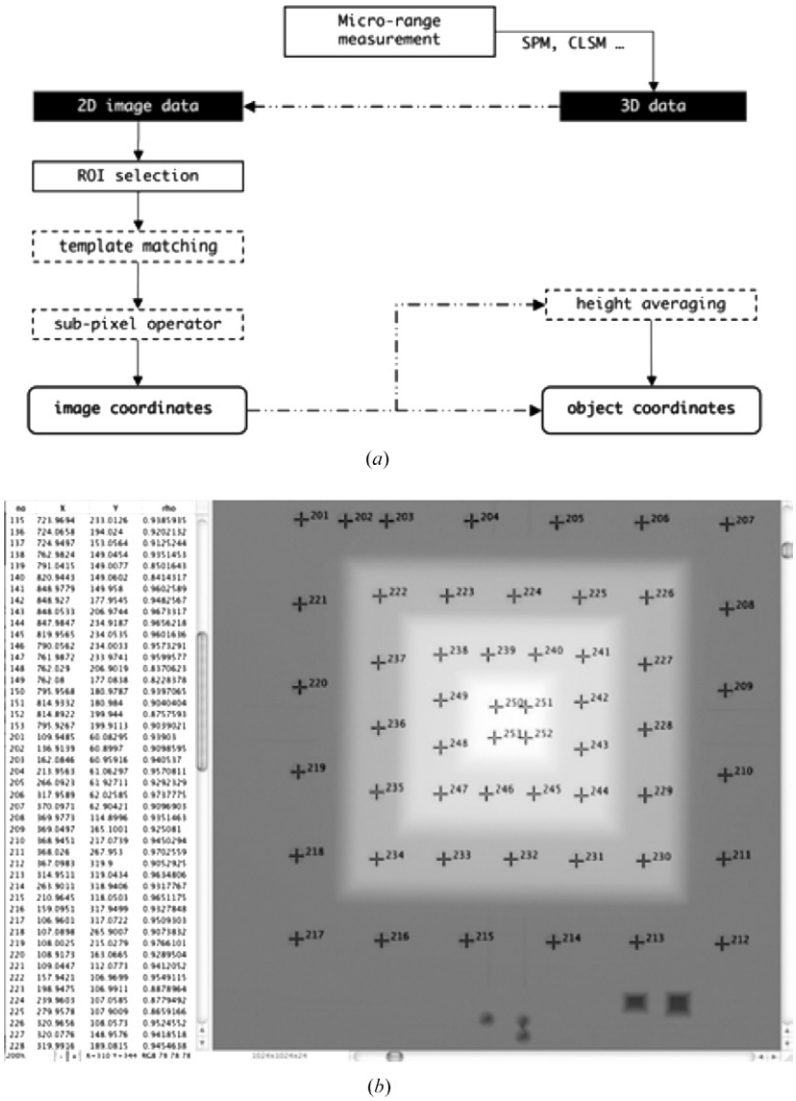

Figure 7. Nanomarker determination and nomenclature. (*a*) Strategy of the nanomarker detection in the digital data (ROI: region of interest). (*b*) Software screenshot with the nanomarker coordinates determined by the software that labels them by their identification number.

determination is done interactively, and can be performed in an automatic, semi-automatic or manual manner. The manual option allows for the visual determination of the approximate location of single nanomarkers, which has proven useful in cases in which a lot of noise or dirt is an issue in the recorded measurement data.

5. Results of 3D landmark-based calibration

5.1. SPM calibration measurements

The first application of the landmark-based 3D calibration method was performed on the reference array FIB03 shown in figure 5. The array consists of three pyramidal structures with 20 μm maximum side length that cover an area of approximately 360 μm^2. On every pyramidal structure, 53 nanomarkers are applied, with a total of 159 landmarks. The reference array was measured by the SIS non-contact SFM (see section 4.1), as shown in figures 6(*a*) and (*b*), then rotated clockwise by 90° and measured again. The nanomarker coordinates of both measurements were determined by template matching with sub-pixel accuracy, according to the strategy of analysis and with the software introduced in section 4.

The extracted object coordinates of the nanomarkers of the array measurement at 90° were registered to the coordinates of the measurement at 0° (table 1). In this case, no reference coordinates **x** are known, and equation (1) has to be adapted to register the two measurement coordinate sets **w** (w_x, w_y, w_z) measured at 0° and **w**′ (w'_x, w'_y, w'_z) measured at 90° as shown in equation (4):

$$\mathbf{w} = \mathbf{R} \cdot \mathbf{M} \cdot \mathbf{S} \cdot \mathbf{w}' + \mathbf{t}. \tag{4}$$

In a first experiment, only rigid parameters, i.e. three rotations and three translations, were used for the least-squares estimation, resulting in a mean point error ξ_p of 166 nm, which is approximately twice the size of a pixel (table 1).

Figure 8(*a*) shows the residues after rigid registration in all three spatial directions depending on their z-value. The correlation between the length of this residual distance

Table 1. Estimated calibration factors after affine 3D registration of nanomarker coordinates measured by SPM before and after clockwise rotation by 90°.

3D registration of nanomarker coordinates of 0 and 90° SPM measurements		
Estimated parameters	3D rigid	3D affine (standard deviation)
Scale c_x	–	0.999 (0.000)
Scale c_y	–	1.002 (0.000)
Scale c_z	–	1.000 (0.001)
Coupling c_{xy}	–	−0.006 (0.000)
Coupling c_{xz}	–	−0.149 (0.001)
Coupling c_{yz}	–	0.154 (0.001)
Mean point error ξ_p (nm)	166	**30**

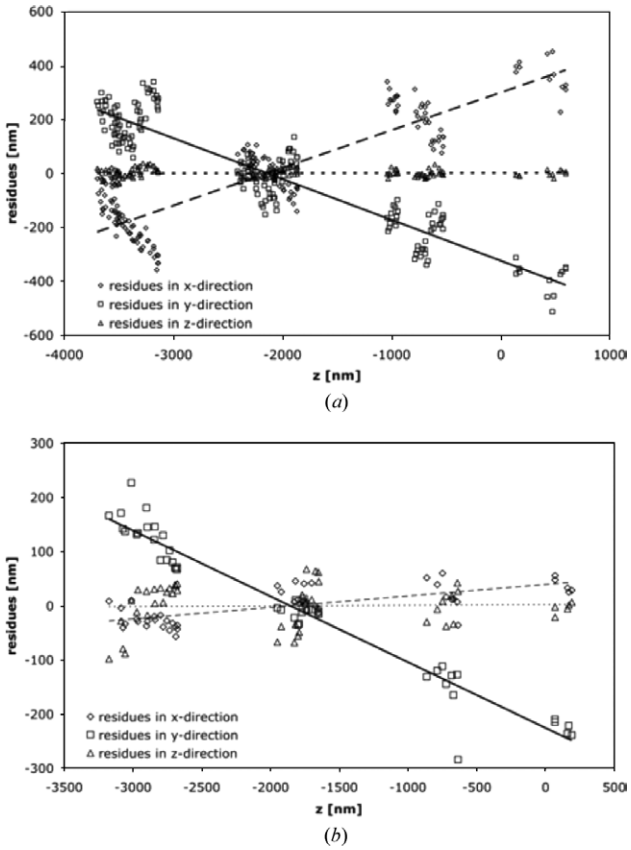

Figure 8. Residues of nanomarker coordinate parameter registration. (*a*) Residues of rigid registration of 0° and 90° SIS nc-SFM measurements (see table 1). (*b*) Residues of rigid registration of SIS nc-SFM measurements and photogrammetric SEM measurements (see table 2).

between two homologous nanomarker coordinates and the particular height position of the same nanomarker can be clearly recognized. This correlation indicates a strong coupling between at least one lateral coordinate axis and the z-axis. Consequentially, when three additional scale and three coupling factors were applied to expand the calibration model for the affine registration by parameter estimation, ξ_p drastically decreased to 30 nm, which corresponds to approximately a third of the size of a pixel in that measurement data (table 1).

The resulting scale factors vary from 0.999 to 1.002, indicating a well-calibrated instrument. The lateral xy-coupling is small, with only a factor of −0.006. However, stronger coupling occurs between the lateral and vertical axes which is proven by the coupling factors c_{xz} of −0.149 and c_{yz} of 0.154, respectively. Both coupling factors, c_{xz} and c_{yz}, are approximately of the same amount, however with opposite algebraic signs.

This result leads to the conclusion that only coupling between mainly one lateral direction and the vertical direction is distorting the measurement, because if a a non-sheared, non-symmetric object in a skewed coordinate system is rotated by 90°, the shearing is rotated as well, here indicated by the altered measurement coordinate system $\mathbf{w}'$ (figure 9). If the measured coordinates of the rotated ($\mathbf{w}'$) and the non-rotated objects ($\mathbf{w}$) are spatially transformed by parameter estimation, then vertical coupling is virtually present for both lateral axes, and it cannot be determined which is the problematic coupling physically affecting the measurement device, in this case the SIS nc-SFM.

5.2. *Correlative measurements of nanomarker coordinates*

In order to determine the problematic coupling factor, e.g., to determine which particular lateral scan axis is non-orthogonal to the z-axis, we photogrammetrically reconstructed the nanomarker object coordinates by SEM for correlative analysis with the coordinates determined by SPM. For this correlative comparison, the nanomarker coordinates of one pyramidal reference structure with 54 circle nanomarkers (an earlier prototype similar to figure 5) were determined by photogrammetric SEM according to [13, 20, 21, 29] as well as by SPM measurement with SIS nc-SFM, as described in section 4.1. The resulting homologous nanomarker coordinates were registered in space by a least-squares parameter estimation, using a rigid transformation model, a non-isotropic scaling model with three scale factors, three coupling models with one coupling factor at a time and, finally, an affine model with three scaling and three coupling factors (table 2).

The power of the 3D calibration model is very nicely shown by an eightfold decrease of the mean point error ξ_p from 83 nm to 10 nm, when applying the affine case using three scale factors and three coupling factors. The main improvement of ξ_p is already achieved if three scale factors and the coupling factor c_{yz} between y- and z-directions are included in the parameter estimation model. Then, ξ_p roughly drops by sevenfold to 13 nm, which is again approximately a third of the size of a pixel in this case, too (table 1). Therefore, the main coupling of the SIS-Nanostation was to be found between y- and z-axes, while only very little coupling occurs between the

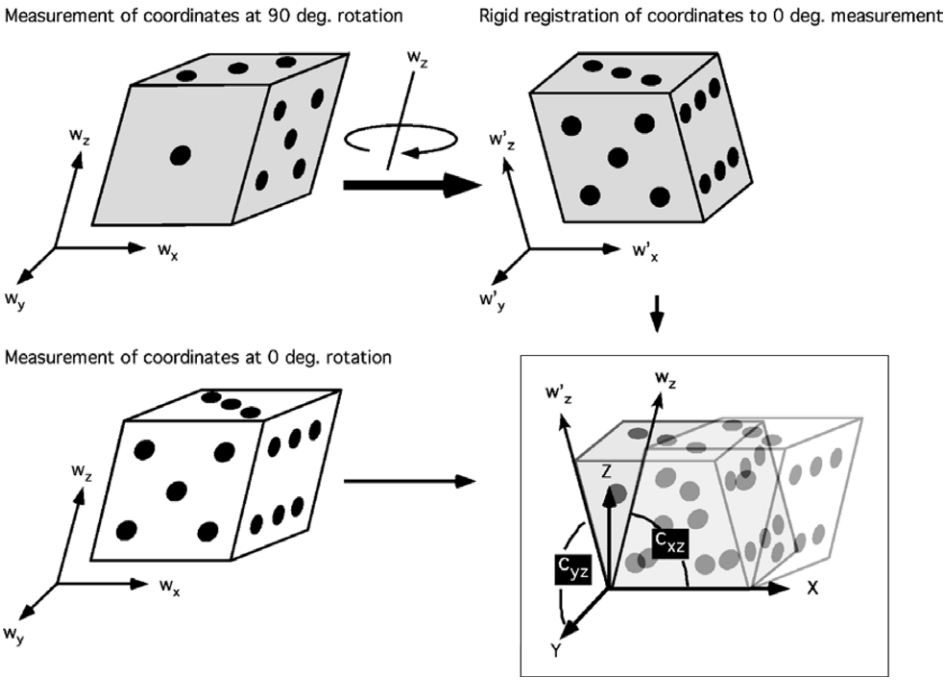

Figure 9. Measurement (represented by a die) in a skewed measurement coordinate system **w** (w_x, w_y, w_z). After the 0° measurement (white die), the object is rotated by 90° and measured again (grey die). When orientating the coordinates represented by the die numbers measured at 90° to those measured at 0° by a rigid 3D registration, no congruency can be achieved (table 1, second column). With respect to the virtual reference system **w**, shear in both lateral directions is apparently present (table 1, third column and figure 8(*a*)) when registering **w**′ to **w** as shown in equation (4)).

Table 2. Correlative analysis of SPM to photogrammetric SEM data by parameter estimation.

3D registration of SPM to photogrammetric SEM nanomarker coordinate measurements						
Parameter	3D rigid	3D scaling	3D *xy*-coupling	3D *xz*-coupling	3D *yz*-coupling	3D affine (standard deviation)
Scale c_x	–	0.998	0.998	0.998	0.999	0.998 (0.000)
Scale c_y	–	0.998	0.998	0.998	0.999	0.999 (0.000)
Scale c_z	–	0.984	0.984	0.983	0.984	0.983 (0.001)
Coupling c_{xy}	–	–	0.001	–	–	0.003 (0.000)
Coupling c_{xz}	–	–	–	0.011	–	0.011 (0.001)
Coupling c_{yz}	–	–	–	–	0.134	0.134 (0.001)
Mean point error ξ_p (nm)	83	82	82	82	**13**	**10**

x- and z-axes, and coupling between the lateral x- and y-axes is almost negligible. The coupling factor c_{yz} determined in the correlative analysis is thus in good agreement with the coupling found in the rotation experiment shown above (table 1), especially when taking into account the small coupling c_{xz} detected between x- and z-directions in the correlative measurement.

6. Discussion

The rather strong coupling of the y- and z-axes may be attributed to the design of the SIS nc-SFM. The z-piezostack might either be mounted tilted in the SIS UltraObjective™, as the fixing of the piezostack is a very delicate work, or it might behave asymmetrically so that a lateral bending of its bottom end, where the cantilever holder is mounted, is induced whenever the piezostack expands in the z-direction. The linear relationship between lateral displacement and height (figure 8(*b*)) suggests, however, that the first assumption of an imprecisely mounted piezostack is more probable, as bending would result in a higher order relationship between lateral displacement and height. The finding itself is new, as this coupling effect had never played a role in the previous investigations of lateral and step height standards with this instrument, and geometry measurements had only been performed at much lower structures where this effect did not become obvious. However, it needs to be stressed that such a coupling between the z-axis and a lateral axis does not affect the results of pitch and step height measurements when measured separately and was thus not detected prior to the measurements with the novel 3D standards. Therefore, the main reason to apply a new 3D calibration method to SPM, and high-resolution scanning microscopy, in general, is to geometrically model the scanning process more accurately (equation (1)) and, thereby, to improve the calibration and overall measurement accuracy. The 3D calibration method

applied is based on homogeneously distributed nanomarkers that can be detected with sub-pixel accuracy by the strategy used (figure 7(*a*)).

The application of FIB itself allows the tailoring of these novel 3D standards largely according to the demands of the user, e.g., by choosing a suitable size for the total array, for the individual pyramids, the number, widths and heights of the cascade terraces and adjusting the design of nanomarkers, i.e. their shape and size, accordingly. The ring-shaped design of the nanomarkers still allows them to be detected optically due to their characteristic appearance, and at the same time enables an accurate coordinate determination in SPM and SEM images by their uniform shape that makes it possible to apply automated image processing including cross-correlation techniques in order to locate them.

This versatility towards usage in several different measurement techniques opens new possibilities for correlative applications, i.e. to obtain a deeper understanding of the individual instruments' performances by a comparative analysis of the data measured by these different instruments at the same 3D standard. As section 5.2 convincingly shows, this might help to detect irregularities of the scan system that otherwise usually remain undiscovered. Correlative analysis is thus a powerful tool that can be exploited well with these standards. Moreover, it does not only allow a better characterization of the measurement system to be reached, but also decreases the uncertainty of the coordinates of the nanomarkers. For instance, the cross-talk of the z-axis on the y-axis in the case of the SIS nc-SFM in section 5.2 may be systematically taken into account in future measurements at these standards as well as at other samples.

We could already show that nanomarker detection is achieved with an uncertainty of a few nanometres, according to the resulting mean point error after 3D parameter estimation with three scale and three coupling factors (tables 1 and 2). Especially with the introduction of all three 3D coupling factors, the mean point error of coordinate measurements could be reduced five- to eightfold in comparative (table 1) or correlative measurements (table 2). This underlines that the introduction of all three coupling factors is reasonable and allows a more adequate description of the scan system. Consequently, the benefit of such a 3D standard compared to using 1D or 2D lateral standards plus step height standards is that it not only allows one to determine the three axes scale correction factors in one step, but also all three coupling factors between the three axes simultaneously. While the coupling c_{xy} between the lateral axes can easily be determined with a 2D standard as well, the determination of the couplings c_{xz} and c_{yz} between the vertical axis and the lateral axes is usually difficult to achieve with the conventional lateral and step heights and, thus, hardly if ever performed by ordinary SPM users. However, as the practical example in section 5.2 demonstrates, the latter might even be much more significant than the coupling within the xy-plane and consequently remains to be taken into account. The inclusion of c_{xz} and c_{yz} determination in this novel 3D calibration scheme enables the user to take these important parameters into account without extra measurement effort and to accomplish a more accurate instrument calibration.

7. Conclusions and outlook

While it could be shown that this novel calibration technique is suited for a rather comfortable calibration of many instruments, its accuracy limits still need to be investigated. It is still too premature to assess whether standards with a design similar to the one shown in this paper allow calibrations of high accuracy, as some of the established high quality standards provide for either the lateral axes or certain height intervals on the vertical axis. Current research activities are therefore directed towards a better understanding of uncertainty contributions originating both from the measurements on these standards and the subsequent data processing. This is done both experimentally, by larger measurement series on different sample designs with several measurement instruments, and theoretically, by taking the results of self-calibration and error-separation techniques into account. Further information to determine the physical cause of the observed results might be gained by using interferometry to monitor the movements of the piezostack. Additionally, it is intended to provide prototypes of this standard to a number of interested partners so that they can test them practically under their measurement conditions. This will encourage a deeper understanding of the measurement and data analysis stability. Ultimately, these investigations are expected to help to better model AFM performance in a 'virtual AFM'. These investigations are, moreover, a prerequisite for the inclusion of such standards as additional or alternative calibration techniques in SPM calibration guidelines such as the present VDI/VDE 2656, which is expected to be complete by late 2006.

Acknowledgments

This project was partly DFG funded (SPP 1159 'StraMNano', KR 987/2–1 and KO 1483/2–1). M Hemmleb provided the software for photogrammetric SEM analysis as well as profound and fruitful discussions, especially in the field of image processing, geometrical analysis and parameter estimation. Thanks are also due to our PTB colleagues M Xu for intensive discussions on the concept of a virtual AFM, error separation and self-calibration strategies and to K Chkhikvadse for data processing and programming. We also thank H Hohenberg, Head of the Microscopy and Micro-Technology Group at the Heinrich-Pette-Insitute, Hamburg, Germany; B Lich and P Faber, FEI Company, Eindhoven, the Netherlands; and R Wepf, S Pagel and S Wessel, Beiersdorf AG, Hamburg, Germany for their support.

References

[1] Wendt U and Wagner D 1994 Synergie von Rasterelektronenmikroskopie und konfokaler Laserrastermikroskopie bei Werkstoffuntersuchungen *Beiträge zur Elektronenmikroskopischen Direktabbildung von Oberflächen (BEDO)* **27** 113–6

[2] Joy D C, Ko Y-U and Hwu J J 2000 Metrics of resolution and performance for CD-SEMs *Proc. SPIE* **3998** 108–15

[3] Yoshida W and Cohen Y 2003 Topological AFM characterization of graft polymerized silica membranes *J. Membr. Sci.* **215** 249–64

[4] Oshima T, Kimoto S and Suganuma T 1970 Stereomicrography with a scanning electron microscope *Photogramm. Eng. Remote Sens.* **36** 874–9

[5] Boyde A 1970 Practical problems and methods in the three dimensional analysis of scanning electron images *Proc. 3rd Ann. Scanning Electron Microscope Symp. (Chicago, 1L)* pp 105–2
[6] Koenig G, Nickel W, Storl J, Meyer D and Stange J 1987 Digital stereophotogrammetry for processing SEM data *Scanning* **9** 185–93
[7] Schattenburg M L and Smith H I 2002 The critical role of metrology in nanotechnology *Proc. SPIE* **4608** 116–24
[8] Wilkening G 2004 Messtechnik für die Nanotechnolgie—eine Herausforderung für die PTB *PTB Mitteilungen* **114** 1–2
[9] Dziomba T, Koenders L and Wilkening G 2005 Standardization in dimensional nanometrology: development of a calibration guideline for scanning probe microscopy *SPIE Europe Optical Design—Optical Fabrication, Testing and Metrology II* **5965**
[10] Boyde A 1973 Quantitative photogrammetric analysis and qualitative stereoscopic analysis of SEM images *J. Microsc.* **98** 452–62
[11] Koenders L, Dziomba T, Thomsen-Schmidt P and Wilkening G 2005 Standards for the calibration of instruments for dimensional nanometrology *Nanoscale Calibration Standards and Methods: Dimensional and Related Measurements in the Micro- and Nanometer Range* ed G Wilkening and L Koenders (Weinheim: Wiley-VCH) pp 245–57
[12] An updated list of commercially available standards can be found on the PTB website http://www.ptb.de/de/org/5/51/514/revstandardsspm.pdf
[13] Ritter M, Hemmleb M, Sinram O, Albertz J and Hohenberg H 2004 A versatile 3D calibration object for various micro-range measurement methods *Proc. 22nd ISPRS Congress (Istanbul)* vol 25 pp 696–701
[14] Gibson C T, Watson G S and Myhra S 1997 Scanning force microscopy—calibrative procedures for best practice *Scanning* **19** 564–81
[15] Henriksen K and Stipp S L S 2002 Image distortion in scanning probe microscopy *Am. Mineral.* **87** 5–16
[16] Zhao X 1995 *PTB-Report F-20* (Bremerhaven)
[17] Jørgensen J F, Jensen C P and Garnaes J 1998 Lateral metrology using scanning probe microscopes, 2D pitch standards and image processing *Appl. Phys.* A **66** 847–52
[18] Garnaes J, Kühle A, Nielsen L and Borsetto F 2005 True three-dimensional calibration of closed loop scanning probe microscope standards for the calibration of instruments for dimensional nanometrology *Nanoscale Calibration Standards and Methods: Dimensional and Related Measurements in the Micro- and Nanometer Range* ed G Wilkening and L Koenders (Weinheim: Wiley-VCH) pp 245–57
[19] Van Den Heuvel F A, Kroon R J G A and Le Poole R S 1992 Digital close range photogrammetry using artificial targets *Int. Arch. Photogramm. Remote Sens.* **29** 222–9
[20] Hemmleb M, Albertz J, Schubert M, Gleichmann A and Köhler J M 1995 Photogrammetrische Bestimmung der Krümmung einer Mikrokantilever-Probe mittels Rasterelektronenmikroskop *Beiträge zur Elektronenmikroskopischen Direktabbildung von Oberflächen (BEDO)* **28** 65–72
[21] Sinram O, Ritter M, Kleindiek S, Schertel A, Hoehenberg H and Albertz J 2002 Calibration of an SEM, using a nano positioning tilting table and a microscopic calibration pyramid *ISPRS Commission V Symp. 2002* pp 210–5
[22] Maurer C R, Maciunas R J and Fitzpatrick J M 1998 Registration of head CT images to physical space using a weighted combination of points and surfaces *IEEE Trans. Med. Imag.* **17** 753–61
[23] Giannuzzi L A, Prenitzer B I and Kempshall B W 2004 *Introduction to Focused Ion Beams* (New York: Springer)
[24] Clampitt R, Mingay P W and Davies S T 1990 Micromachining with focused ion beams *Sensors Actuators* A **25** 15–20
[25] Overwijk M H F and Van Den Heuvel F C 1993 Focused-ion beam-induced tungsten deposition: theory and experiment *Nucl. Instrum. Methods Phys. Res.* B **80–81** 1324–7
[26] Dziomba T, Häßler-Grohne W, Bosse H, Danzebrink H-U and Wilkening G 2003 Influence of nanostandard properties on calibration procedures of SPMs *Proc. Euspen Int. Topical Conf. (Aachen, Germany)* ed M Weck and H Kunzmann pp 491–4
[27] Dai G, Pohlenz F, Danzebrink H-U, Hasche K and Wilkening G 2005 DSP-based metrological scanning force microscope with direct interferometric position measurement and improved measurement speed *Nanoscale Calibration Standards and Methods: Dimensional and Related Measurements in the Micro- and Nanometer Range* ed G Wilkening and L Koenders (Weinheim: Wiley-VCH) pp 245–57
[28] Dai G, Pohlenz F and Danzebrink H U *et al* 2004 Metrological large range scanning probe microscope *Rev. Sci. Instrum.* **75** 962–9
[29] Ritter M, Hemmleb M, Lich B, Faber P and Hohenberg H 2006 SEM/FIB stage calibration with photogrammetric methods *ISPRS Commission V Symp. 2006 (Int. Archives of Photogrammetry, Remote Sensing and Spatial Information Sciences)* Vol XXXVI Part 5